Higgs boson production at a photon linear collider

Douglas L. Borden, Daniel A. Bauer, and David O. Caldwell
Physics Department, University of California, Santa Barbara, California 93106
(Received 5 March 1993)

The collision of high-energy, high-intensity photon beams would provide novel opportunities for particle physics. These beams could be obtained at a linear e^+e^- collider via Compton backscattering using high-powered lasers. The resulting photon linear collider offers highly polarized beams, large luminosities, and a variable luminosity spectrum. We examine the potential of such a machine to explore the Higgs sector of the standard model. We find a photon linear collider with $\sqrt{s} \approx 250$ GeV to be an excellent tool to search for an intermediate-mass Higgs boson, with the polarized photon beams being a particular asset, as they can be used to suppress backgrounds while enhancing the signal. In searching for intermediate-mass standard model Higgs bosons, a signal in excess of 10σ over the entire intermediate mass region is possible with even moderate luminosity. Even more important is the application of a photon linear collider to measurement of the two-photon width of the Higgs boson, a measurement which gives crucial information about the nature of spontaneous symmetry breaking. We calculate that a photon linear collider with energy tuned to the Higgs boson mass allows a measurement of the two-photon width of the Higgs boson with a statistical precision of better than 10% over most of the intermediate- and heavy-mass range.

PACS number(s): 14.80.Gt, 12.15.Ji, 13.10.+q, 14.80.Am

I. INTRODUCTION

The exploration of the spontaneous symmetry-breaking sector of the standard model is sure to provide one of the most active pursuits in particle physics over the next decades. Searches at the CERN e^+e^- collider LEP have found no evidence for the standard model Higgs boson up to 48 GeV, with somewhat lower mass limits on neutral supersymmetric Higgs bosons [1]. LEP II should extend these limits up to nearly the mass of the Z [2]. For Higgs boson masses above twice the Z mass almost certain detection is assured at the Superconducting Super Collider (SSC) or CERN Large Hadron Collider (LHC) in the "gold plated" decay mode $H \rightarrow ZZ \rightarrow 4$ leptons [2]. It is the intermediate-mass Higgs boson, in the range $80 < M_H < 2M_W$, which is the most difficult to access experimentally. In this mass range the Higgs boson decays predominantly to $b\bar{b}$. Discovery of an intermediate-mass Higgs boson at a hadron collider must occur through the decay of the Higgs boson to two photons, as the QCD backgrounds there make it impossible to use the $b\bar{b}$ decay channel [2]. At the SSC or LHC this $\gamma\gamma$ discovery channel seems tenable for Higgs boson masses above ~ 120 GeV, but studies indicate that only a detector with superb electromagnetic calorimetry and photon angle resolution will be capable of extending the range any further down in mass. Associated W production of the Higgs boson (resulting in the decay mode $WH \rightarrow l\nu\gamma\gamma$) allows for significant background suppression, extending the accessible range all the way down to 80 GeV, but suffers from an abysmally low rate [3].

High-energy linear e^+e^- colliders provide a clean environment in which to explore the intermediate-mass region. Production of an intermediate-mass Higgs boson at an e^+e^- collider proceeds through either the bremsstrahlung process ($e^+e^- \rightarrow ZH$) [4] or through WW fusion ($e^+e^- \rightarrow \nu\bar{\nu}H$) [5]. At center-of-mass energies below about 500 GeV the bremsstrahlung process dominates, while above that the WW fusion process is most important. The absence of an energy constraint in WW fusion limits the Higgs boson mass discovery region accessible at high-energy ($\sqrt{s} > 500$ GeV) linear colliders to greater than about 130 GeV. At lower $\sqrt{s}$ machines the discovery potential is better, and the mass region accessible extends all the way down to LEP-II limits. Discovery of a Higgs boson with a mass near 90 GeV is more difficult as it requires tagging of the b-quark final states to reduce the background from $e^+e^- \rightarrow ZZ$ [2].

The intermediate-mass region, as difficult experimentally as it is, is a particularly intriguing one theoretically. Weak scale supersymmetry, one of the most favored extensions to the standard model, predicts a wealth of Higgs phenomenology in the intermediate-mass range. In the minimal supersymmetric extension to the standard model (MSSM), one neutral Higgs boson *must* have a mass below ~ 140 GeV, with others appearing in this range over much of supersymmetric parameter space [2,6]. The theoretical importance of this mass region underscores the importance of ensuring full experimental coverage. A $\gamma\gamma$ linear collider provides an alternative method to search for an intermediate-mass Higgs boson, through resonant $\gamma\gamma \rightarrow H \rightarrow b\bar{b}$ production. As such it is complementary to hadron and e^+e^- machines, being sensitive to different models and couplings.

Furthermore, a $\gamma\gamma$ linear collider permits a direct measurement of the two-photon width of the Higgs boson, one of the most important properties to determine in studying a Higgs boson. The coupling of the Higgs boson to two photons involves loops where any charged fermion or boson with couplings to the Higgs boson must contribute, as shown in Fig. 1. Thus, a measurement of the

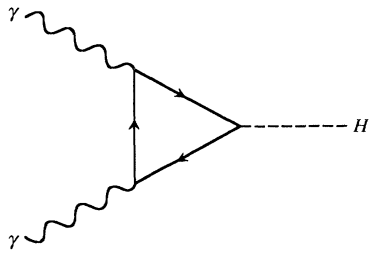

FIG. 1. The coupling of the Higgs boson to two photons. The coupling proceeds through loops of charged particles which couple to the Higgs boson.

two-photon width is quite sensitive to new physics even at higher mass scales [7]. Supersymmetric models, technicolor models, and other extensions of the standard model with more complicated Higgs boson sectors all predict two-photon couplings which are, in general, very different from that of the standard model [2,8]. As examples we consider two simple extensions to the standard model: an unconstrained two Higgs doublet model and the MSSM.

Adding a second Higgs doublet to the standard model results in five physical scalars: two neutral scalar Higgs bosons (h^0,H^0), a neutral pseudoscalar Higgs boson (A^0), and two charged Higgs bosons ($H^{\pm}$) [2]. Plotted in Fig. 2 is the $h^0 \to \gamma\gamma$ width as a function of tanβ (the ratio of Higgs boson vacuum expectation values) for different values of the neutral scalar Higgs boson mixing angle α. Clearly, the two-photon width can differ from that in the standard model by several orders of magnitude.

The MSSM, a popular extension to the standard model, is a constrained two-Higgs doublet model. In the MSSM, once a supersymmetry scale is chosen, the masses of all the Higgs bosons, and most of their decay widths, are determined by just two linearly independent parameters, traditionally chosen as M_A and tanβ [2,6]. Since

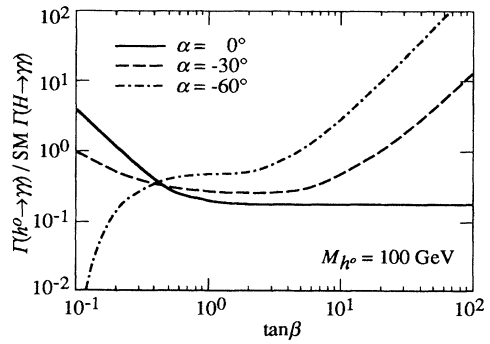

FIG. 2. The Higgs boson (h^0) two-photon partial width in an extension to the standard model with two Higgs doublets, for $M_{h^0}=100$ GeV. tanβ is the ratio of Higgs boson vacuum expectation values, and α is the neutral scalar Higgs boson mixing angle. The other physical Higgs bosons are assigned the following masses: $M_{H^{\pm}}=100$ GeV; $M_{A^0}=300$ GeV; $M_{H^0}=500$ GeV. The partial width is normalized to the standard model value.

charginos enter into the $H\gamma\gamma$ loop, their mass parameters must be chosen as well to predict the two-photon partial width of an MSSM Higgs boson. Plotted in Fig. 3 is the $h^0 \to \gamma\gamma$ width in the MSSM, as a function of M_A and tanβ, normalized to the standard model value [9]. A supersymmetry scale of 1 TeV is chosen and the chargino mass parameters M and μ are taken to be 300 and 100 GeV, respectively. For $M_A < 110$ GeV and tan$\beta > 2$, the $h^0 \to \gamma\gamma$ width is a sensitive function of the MSSM parameters; measuring it would severely constrain the model.

In the large M_A, large tanβ region of Fig. 3, the h^0 mass saturates at its maximum value (~ 110 GeV for the assumed parameters), and its $\gamma\gamma$ width is near that of the standard model—the $\sim 20\%$ difference is due to the presence of the charginos. If, instead, the charginos were to be taken to be very heavy, then, in this region, the $\gamma\gamma$ width would be within a few percent of the standard model value. A precision measurement of the two-photon width of such a Higgs boson would be sensitive to the presence of light charginos in the supersymmetric spectrum. It should be noted that observation of the $\gamma\gamma$ decay of the h^0 for M_A below ~ 200 GeV is not possible at the SSC or LHC, as the $h^0 \to \gamma\gamma$ branching ratio is very small [10].

In this paper we explore in detail the ability of a photon linear collider (PLC) to discover an intermediate-mass Higgs boson and to measure the two-photon width of a Higgs boson, of intermediate or heavy mass, once one is found. In Sec. II we review the scheme for constructing a $\gamma\gamma$ collider based on Compton backscattered laser beams. In Sec. III we consider the relevant cross sections for two-photon production of Higgs bosons and possible backgrounds. In Sec. IV we assess the capability of a PLC to search for an intermediate-mass Higgs boson, and present the results of Monte Carlo simulations of a Higgs bosons search at a photon linear collider. In Sec.

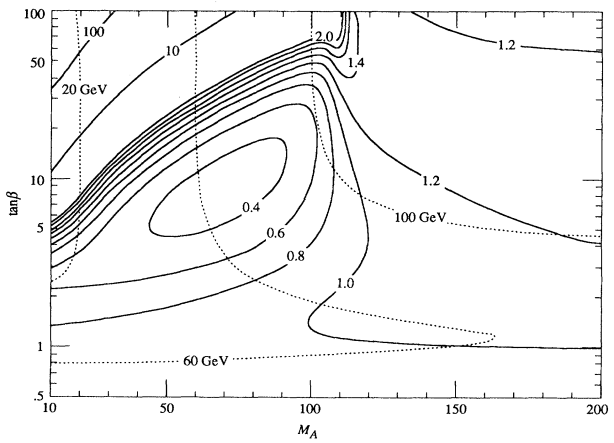

FIG. 3. The $h^0 \to \gamma\gamma$ partial width in the MSSM [9]. The dashed lines are contours of constant h^0 mass; the solid lines are contours of constant ratio: $\Gamma(h^0 \to \gamma\gamma, \text{MSSM})/\Gamma(H \to \gamma\gamma, \text{SM})$. The common sfermion mass is taken to be 1 TeV and the chargino mass parameters M and μ are chosen as 300 and 100 GeV, respectively.

V we examine a PLC's ability to measure the $\gamma\gamma$ width of an intermediate- or heavy-mass Higgs boson, again presenting the results of a Monte Carlo simulation. Section VI is a summary and conclusion.

II. PHOTON LINEAR COLLIDERS

The Compton collider scheme is described elsewhere [11–13], so we only briefly review here the physics of colliding Compton backscattering laser beams to establish the notation and formalism.

A. Compton scattering

A laser of frequency w_0 and circular polarization λ_γ is focused on a linac electron beam of energy E_b and longitudinal polarization λ_e a few centimeters upstream of the interaction point (IP). In the collision of a laser photon and a linac electron, a high energy photon of energy ω and circular polarization λ is emitted at an angle θ_γ to the original direction of the electron beam, along with the scattered electron of energy $E=E_b-\omega$, emitted at an angle θ_e. The Compton kinematics are characterized by the dimensionless variable x:

$$x\equiv\frac{4E_b w_0}{m_e^2}\approx 15.3\left[\frac{E_b}{\text{TeV}}\right]\left[\frac{w_0}{\text{eV}}\right] \tag{1}$$

and by the polarization of the linac electrons and laser photons [11]. In general, the backscattered photon energies increase with x; the maximum photon energy is given by $\omega_{\max}=E_b x/(x+1)$ [11]. In order to prevent reconversion of a high-energy photon into an e^+e^- pair in a collision with a laser photon farther along in the laser pulse, this x parameter must be kept below 4.83 [12]. We will work at an x value of 4.80 in this paper.

Figure 4 shows the photon energy distribution for unpolarized Compton scattering. The backscattered photons are distributed approximately uniformly in energy from zero to near the maximum, where the distribution peaks. The scattering angles of the electron and photon are small, but finite, and correlated with energy. The photon scattering angle, also shown in Fig. 4, is given by

$$\theta_\gamma(\omega)=\theta_0\left[\frac{\omega_{\max}}{\omega}-1\right]^{1/2},$$
$$\theta_0=\frac{m_e\sqrt{x+1}}{E_b}\approx\frac{0.511\sqrt{x+1}}{E_b/\text{TeV}}\ \mu\text{rad}\ . \tag{2}$$

Note that for beam energies of a few hundred GeV, a typical photon scattering angle is a few microradians. The electrons scatter forward with scattering angles typical of those of the highest energy photons.

Polarizing the linac electrons and laser photons not only provides polarized backscattered photons, but also allows one to tailor the photon energy distribution to one's needs. Colliding like-handed electrons and photons results in a flat distribution of backscattered photons; colliding oppositely handed electrons and photons results in a peaked distribution of backscattered photons. In both cases the resulting photons are highly polarized, as shown in Fig. 5 [11].

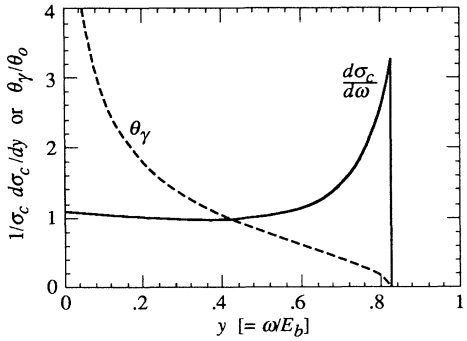

FIG. 4. Energy spectrum and scattering angle of high-energy photons from Compton backscattering.

B. $\gamma\gamma$ collisions

In a photon linear collider the high-energy photon beams produced from Compton backscattering collide at the interaction point. Assuming round linac beams with a Gaussian density profile (and "radius" σ_e), we define the *effective luminosity*

$$L_{\text{eff}}\equiv\frac{N_\gamma^2 f}{4\pi\sigma_e^2}=\frac{(\kappa N_e)^2 f}{4\pi\sigma_e^2}=\kappa^2 L_{ee}\ , \tag{3}$$

where N_e is the number of electrons in each bunch, κ is

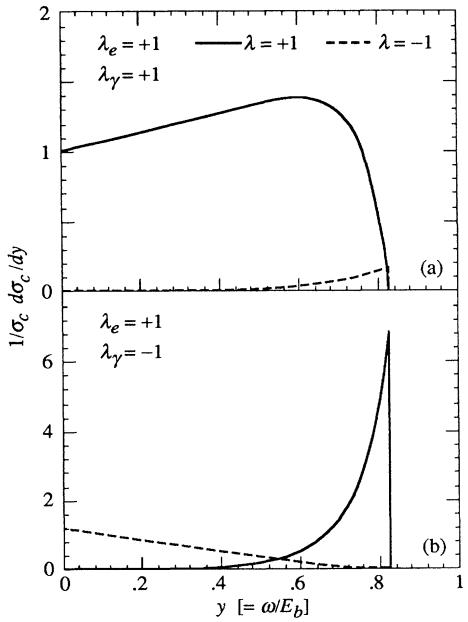

FIG. 5. Energy spectrum of backscattered photons from Compton scattering with polarized beams. The solid line in each plot is the spectrum of positive helicity photons and the dashed line is that of negative helicity photons.

the fraction of electrons in each bunch that Compton scatter in the laser pulse (≈ 0.5), f is the collision frequency, and L_{ee} denotes the luminosity of the underlying ee machine given purely by geometric considerations (i.e., beam-beam effects are ignored). Since $L_{\rm eff}$ does not take into account the finite scattering angles of the photons, it serves only as an upper limit to the possible photon-photon luminosity; in general, $L_{\gamma\gamma}=(0.1-1)L_{\rm eff}$, depending on the monochromaticity of the luminosity spectrum required.

Equation (3) indicates that $L_{\rm eff}$, and therefore $L_{\gamma\gamma}$, is less than L_{ee}. However, because of the absence of beam-beam effects at the interaction point (IP), the $\gamma\gamma$ luminosity can actually be higher than the possible e^+e^- luminosity for many linear collider designs [12,14]. The expression for L_{ee} seems to indicate that achieving arbitrarily high e^+e^- luminosities is possible merely by making the electron and positron bunches ever more dense. In reality the use of such extremely dense bunches leads to highly disruptive effects at the IP. As the beams pass through each other they are so distorted by the electromagnetic fields in the opposing bunch that they "blow up" long before they have fully collided, resulting in a drastic decrease in the true e^+e^- luminosity. In order to avoid this effect, e^+e^- linear colliders must be operated with only moderate beam currents, limiting the e^+e^- luminosity to a few$\times 10^{33}$ cm^{-2}s^{-1} [15]. When the machine is operated as a $\gamma\gamma$ collider such beam-beam effects are greatly reduced [12,14]. If the accelerating structure of the collider is capable of carrying very high currents, then such a machine can be operated at very high bunch densities. The result is that the ensuing $\gamma\gamma$ luminosity can be larger than the possible e^+e^- luminosity. Superconducting colliders are being designed to operate with high beam loads ($\sim 10^{11}$ e^-/bunch), high repetition rates (~ 8 kHz), and rather large spot sizes (~ 100 nm) [16], making it possible to contemplate *effective* PLC luminosities ($L_{\rm eff}$) of $\sim 10^{34}$ cm^{-2} s^{-1}. In this paper, when we consider event rates, we assume a conservative value of 2×10^{33} cm^{-2}s^{-1} for the effective luminosity, leading to 20 fb^{-1} of integrated luminosity in one "year" (10^7 sec).

The energy distribution of the colliding photon beams is not monochromatic, so the resulting luminosity distributions is as important to understand as the total luminosity. Because of the small, but finite, photon scattering angles, the luminosity distribution depends sensitively on the conversion distance (distance from the conversion point, where the laser pulse intersects the electron beam, to the interaction point) and the size and shape the electron beam would have had at the interaction point in the absence of a backscattering laser. Again assuming round Gaussian linac beams, the luminosity spectrum is characterized by the geometrical factor ρ, the ratio of the intrinsic transverse spread of the photon beam to that of the original electron beam:

$$\rho \equiv \frac{z\theta_0}{\sqrt{2}\sigma_e} \approx 3.61\sqrt{x+1}\left[\frac{z}{\rm cm}\right]\left[\frac{E_b}{\rm TeV}\right]^{-1}\left[\frac{\sigma_e}{\rm nm}\right]^{-1}, \tag{4}$$

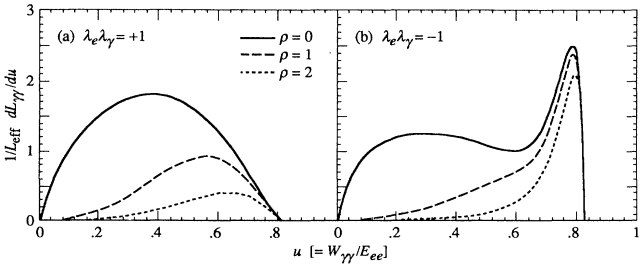

FIG. 6. $\gamma\gamma$ luminosity distributions for two polarization combinations and various values of ρ.

where z is the conversion distance and θ_0 is defined in Eq. (2) [11]. The ρ parameter measures the growth of the IP spotsize due to the photon scattering angles. For $\rho \ll 1$, the total luminosity is equal to the effective luminosity. As ρ increases the monochromaticity of the luminosity distribution improves (because the lowest energy photons, scattering at the largest angles, end up outside the IP), but the total luminosity decreases.

Figure 6 shows polarized $\gamma\gamma$ luminosity distributions, indicating that increasing ρ (achieved in practice by increasing the conversion distance) decreases the low-mass luminosity, which results in more monochromatic collisions. For simplicity we have ignored the effects on the luminosity distribution of secondary photons resulting from multiple scattering of the electrons in the laser photon pulse.

III. CROSS SECTIONS

A. Signal cross section

For Higgs boson masses up to about 300 GeV, the beam energy spread of a PLC is much greater than the total width of the Higgs boson, so the number of $H\to X$ ($X=b\bar{b}$, WW, ZZ) events expected is

$$N_{H\to X}=\left.\frac{dL_{\gamma\gamma}}{dW_{\gamma\gamma}}\right|_M \frac{4\pi^2\Gamma(H\to\gamma\gamma)B(H\to X)}{M^2}(1+\lambda_1\lambda_2)\ , \tag{5}$$

where $B(H\to X)$ is the branching ratio of the Higgs boson into final state X, λ_1 and λ_2 are the helicity states of the initial photons, and $W_{\gamma\gamma}$ is the two-photon invariant mass. Note that since the Higgs boson is a spin-0 boson, the initial photons must be in a $J_z=0$ state.

Figure 7 shows the production rate of $\gamma\gamma\to H\to b\bar{b}$, WW, ZZ events, where $\lambda_1\lambda_2=1$ and a typical value of 4×10^{-2} fb^{-1}/GeV is taken for $dL_{\gamma\gamma}/dW_{\gamma\gamma}$. The relevant widths and branching ratios can be found in Ref. [2]. A top-quark mass of 150 GeV is assumed.

For Higgs boson masses below 140 GeV the dominant decay is to $b\bar{b}$, and that mode is still non-negligible up to about 150 GeV. Above 150 GeV vector boson final states dominate, with one of the vector bosons being virtual below threshold. WW decays are predominant, but the rate into ZZ is appreciable.

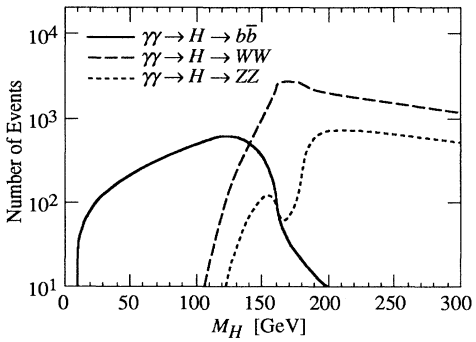

FIG. 7. Production rate of standard model Higgs bosons into the three exclusive final states relevant for the intermediate- and heavy-mass regions. A value of 4×10^{-2} fb^{-1}/GeV is assumed for $dL_{\gamma\gamma}/dW_{\gamma\gamma}$.

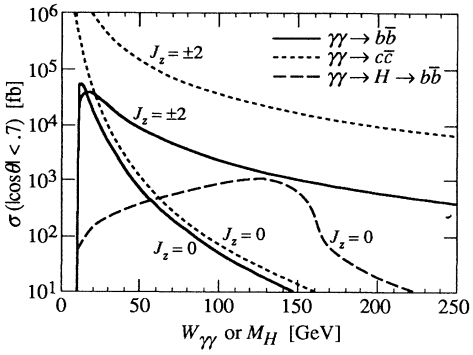

FIG. 8. Cross sections for $\gamma\gamma \to b\bar{b}$, $\gamma\gamma \to c\bar{c}$, and $\gamma\gamma \to H \to b\bar{b}$.

B. Background cross sections: Intermediate-mass region

In the intermediate-mass region, the dominant background to $\gamma\gamma \to H \to b\bar{b}$ will be continuum production of heavy quarks, assuming vertexing techniques can be used to eliminate backgrounds from light quarks. These backgrounds are quite large, but can be actively suppressed by exploiting the polarization dependence of the cross sections. Far above threshold, the $\gamma\gamma \to f\bar{f}$ cross section is dominated by initial photons in the $J_z = \pm 2$ helicity state. Recalling that the signal results from the $J_z = 0$ channel, polarized collisions can be used to enhance the signal while simultaneously suppressing the background. Furthermore, continuum production of fermion pairs occurs preferentially at large dip angle ($|\cos\theta| \approx 1$), while the signal events are distributed uniformly in $\cos\theta$. Thus, a cut on $|\cos\theta|$ serves further to enhance the signal over background.

Direct comparison of the continuum background cross sections with the resonant signal cross section is difficult. As is indicated in Eq. (5), the event rate of signal events is proportional to $dL_{\gamma\gamma}/dW_{\gamma\gamma}$, while the event rate for the continuum background is proportional to the total luminosity $L_{\gamma\gamma}$. In comparing signal (S) to background (B) cross sections, we have chosen to normalize the signal cross sections as if $(dL_{\gamma\gamma}/dW_{\gamma\gamma})_S = (L_{\gamma\gamma})_B/(10\text{ GeV})$. This is typical of experimental situations at a PLC, and is equivalent, for the purposes of comparison, to assuming that the experimental resolution on reconstructing the Higgs boson mass is 10 GeV.

Figure 8 shows two-photon cross sections for $b\bar{b}$ and $c\bar{c}$ production in polarized collisions [17], indicating the very large suppression of this cross section possible by using polarized photons in the $J_z = 0$ state. Note that a cut of $|\cos\theta| < 0.7$ has also been applied. For comparison, the Higgs boson signal cross section is superimposed, with the normalization as discussed above. It is clear that high polarization (to suppress continuum backgrounds) and excellent flavor tagging (to reduce further the $c\bar{c}$ background) will be crucial in extracting a Higgs boson signal from the background.

In addition to the direct $\gamma\gamma \to q\bar{q}$ backgrounds, in some experimental situations there will also be a resolved photon contribution to heavy quark production [18]. In such a process one or both initial state photons emit a virtual gluon, leaving a spectator jet remnant; heavy quark production then proceeds through photon-gluon or gluon-gluon fusion. At high-energy $\gamma\gamma$ colliders ($\sqrt{s} \geq 500$ GeV) resolved processes dominate over direct processes for heavy quark production in the intermediate-mass region [19]. For the lower-energy colliders we will consider, however, resolved processes should be unimportant. Resolved photon cross sections are large when the invariant mass of the produced heavy quark pair is much less than the invariant mass of the initial two-photon system; the remnant jet carries off most of the available energy. We will consider collider energies such that the mass of the Higgs boson signal is never less than approximately $\frac{1}{3}$ of the highest possible two-photon invariant mass. In this kinematic configuration, it is expected that the resolved photon contribution will be less than the direct contribution. Furthermore, even this small resolved photon contribution to the background can most probably be removed. Monte Carlo studies indicate that it should be possible to tag the spectator jet and therefore reject the resolved background, even if the detector is blind above $|\cos\theta| = 0.985$. We therefore do not include resolved processes as a background in our analysis.

C. Background cross sections: $M_H \approx M_Z$

In searching for a Higgs boson with mass near that of the Z there may be substantial $\gamma\gamma$ flux at masses greater than 91 GeV, leading to other backgrounds which must be considered. These backgrounds represent the production of a $Z + X$ final state with X going undetected and the Z decaying to a $b\bar{b}$ pair. Before discussing these backgrounds, it should be noted that resonant production of a Z (i.e., $\gamma\gamma \to Z$) is *not* a background to $\gamma\gamma \to H$. By Bose symmetry, two massless spin-1 objects do not couple to a spin-1 resonance (the Yang-Landau theorem [20]). Consequently, the coupling of the Z to two real photons is identically zero. This is an important advantage of a photon linear collider.

Two potential backgrounds which might fake the presence of a 91 GeV Higgs boson are $\gamma\gamma \to \gamma Z \to \gamma b\bar{b}$ with the photon disappearing down the beam pipe, and $\gamma\gamma \to ZZ \to \nu\bar{\nu}b\bar{b}$. At high energies these cross sections are appreciable, but below $W_{\gamma\gamma} = 300$ GeV they are quite small and contribute negligibly to the $b\bar{b}$ background near 91 GeV [21].

The dominant potential background faking the presence of a Z-mass Higgs boson is not a two-photon background, but rather is due to the presence of the residual electrons left over from the original Compton backscatter. Recall that these electrons follow very nearly their original path and so intersect the oncoming high-energy photon beam at the interaction point. The process $e\gamma \to eZ \to eb\bar{b}$ is then possible, and the final-state electron is preferentially backscattered down the beam pipe, where it goes undetected. Monte Carlo studies show that the event rate for this process is two to three orders of magnitude larger than that from Higgs boson production. In order to minimize this background, it will be essential to displace transversely the residual electrons far enough from the interaction point so as to reduce the $e\gamma$ luminosity by several orders of magnitude. This can be accomplished with a strong magnetic field around the interaction point. Displacing the electrons, of course, requires a finite distance between the conversion point and the interaction point. Ensuring enough separation of the electrons from the photons requires that the ρ parameter be not less than ~ 0.5.

There is one other non-negligible background relevant for Higgs boson masses near that of the Z: $\gamma\gamma \to f\bar{f}Z$, where the $f\bar{f}$ go down the beampipe and $Z \to b\bar{b}$ [22]. This is the untagged "two-fermion" equivalent of the virtual bremsstrahlung two-photon process at e^+e^- colliders. The cross section (summed on final state fermions) is shown in Fig. 9. Note that this cross section should not be compared directly with those of Fig. 8 because the integration range in $W_{\gamma\gamma}$ is necessarily different. The relative size of this background compared to a Higgs boson signal will be discussed later.

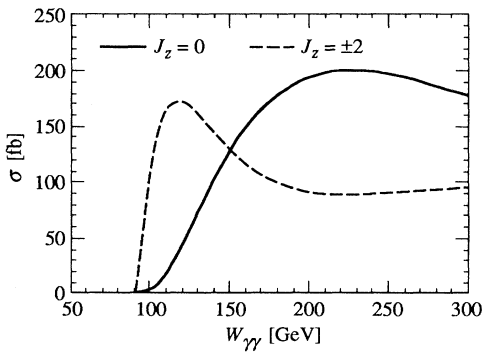

FIG. 9. The untagged $\gamma\gamma \to f\bar{f}Z \to f\bar{f}b\bar{b}$ cross section, summed on final-state fermions. A Weizsacker-Williams-like "equivalent fermion approximation" is used for the two-fermion flux [22].

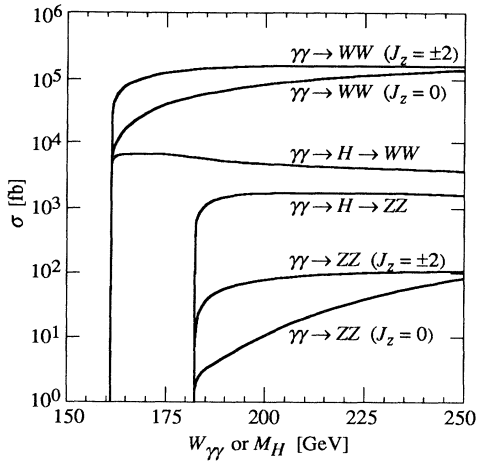

FIG. 10. Cross sections for $\gamma\gamma \to WW, ZZ$ and $\gamma\gamma \to H \to WW, ZZ$. Only real vector bosons are included.

D. Background cross sections: Heavy-mass region

Above 150 GeV the dominant Higgs boson decay is to WW, with one of the W's virtual below 162 GeV. The cross section for $\gamma\gamma \to WW$ is shown in Fig. 10 [23], along with resonant $\gamma\gamma \to H \to WW$ production for comparison; only real W's are included. The continuum cross section is very large, and does not display the severe polarization dependence that the fermion pair-production cross section did. Also, no significant enhancement of signal-to-noise results from restricting the production angle. The WW final state will be a difficult one to use for doing Higgs physics.

Fortunately, the ZZ (or ZZ^*) decay channel can be utilized. The Higgs boson has a branching fraction into this channel of approximately $\frac{1}{3}$ (for real Z's), while the standard model cross section for $\gamma\gamma \to ZZ$ is small, as can be seen from Fig. 10 [21]. Hadronic decays of the Z bosons predominate, but the huge $\gamma\gamma \to WW$ cross section results in a large number of "fake ZZ" events (both W's being misidentified as Z's), so that unambiguous tagging of ZZ requires at least one Z to decay leptonically. The combinatoric background to the $ZZ \to Zll$ final state is negligible [24].

IV. HIGGS BOSON SEARCH AT A PLC

We concentrate on exploring the mass region between 80 and 150 GeV, where the dominant decay of the Higgs is to $b\bar{b}$. The search for an intermediate-mass Higgs boson requires a luminosity distribution dominated by $J_z = 0$ collisions and covering the region of interest. In principle this could be accomplished in either of two ways: by utilizing the peaked luminosity spectrum of Fig. 6(b) and sweeping the beam energy across the region of interest, or by utilizing the broad luminosity spectrum of Fig. 6(a) at a fixed beam energy. While the former choice is superior for covering a small mass region, it results in insufficient luminosity when trying to cover the entire intermediate-mass region. We therefore choose the

broad luminosity distribution resulting from a polarized linac and laser in the $\lambda_e\lambda_\gamma > 0$ configuration. A linac beam energy of 125 GeV is a good choice for the underlying ee machine, as it provides both high $\gamma\gamma$ luminosity and high photon polarization over the entire region of interest. The ρ parameter should be chosen small enough so that there is sufficient luminosity at low invariant mass, but large enough so that sufficient transverse separation of the electron and photon beams at the IP can be obtained to eliminate $e\gamma \to eZ \to (e)b\bar{b}$ as a background. A ρ value of 0.6 satisfies both these criteria and is the choice adopted here.

The luminosity distributions of Fig. 6, and the photon energy distributions of Fig. 5, assume 100% linac polarization; in practice, this will not be possible to achieve, although lasers can easily be polarized to near 100%. Present work, however, indicates that electrons with polarization as high as 90% will be available for use in linear colliders [25,26]. Figure 11 shows the luminosity distribution resulting from the machine parameters described above, using electron beams with 90% polarization, and assuming 20 fb^{-1} of integrated effective luminosity.

Plotted in Fig. 12 are expected event rates for both the signal and background processes, given the luminosity distribution of Fig. 11. It is found that the highest statistical significance of the Higgs boson signal is obtained with a cut on production angle of approximately $|\cos\theta| < 0.7$; this is the reason for the cut indicated in Fig. 8. This cut is also employed here. The data are binned in 10 GeV bins and it is assumed that all the Higgs boson events fall in one bin.

It is obvious that excellent b tagging and charm rejection by vertexing and particle identification in the detector will be necessary to suppress the background from charm and light quarks. Note that keeping the charm-to-bottom ratio as low as possible will be more important than tagging a very high fraction of the $b\bar{b}$ events, as unsuppressed charm is potentially the dominant background. Bringing the $c\bar{c}$ background below the $b\bar{b}$ background requires that the acceptance ratio of $c\bar{c}$ to $b\bar{b}$ events must be below $\frac{1}{16}$. Although this is quite difficult to achieve with present vertex detectors, preliminary

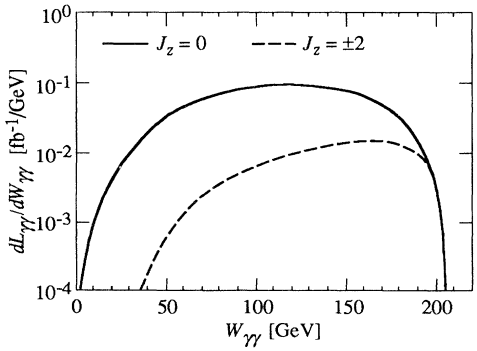

FIG. 11. The $\gamma\gamma$ luminosity distribution to be used in a search for intermediate-mass Higgs bosons. 20 fb^{-1} of integrated effective luminosity is assumed.

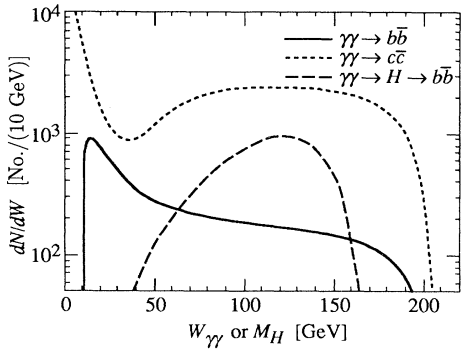

FIG. 12. Expected event rates for a search for an intermediate-mass Higgs boson; a cut of $|\cos\theta| < 0.7$ is included.

studies indicate that pixel vertex detectors planned for use at the next linear collider should be capable of such discrimination while still allowing high $b\bar{b}$-tagging efficiency [27]. Specifically, it is reasonable to assume a 50% $b\bar{b}$-tagging efficiency with a 5% $c\bar{c}$-to-$b\bar{b}$ acceptance ratio. The expected statistical significance of the Higgs boson signal, given these assumptions, is plotted in Fig. 13. This plot also assumes that the resolution for reconstructing the invariant mass of a two-jet event is Gaussian with a full width at half maximum (FWHM) equal to 10% of the total energy.

While the above analysis serves as a good first-order determination of the potential for a Higgs boson search at a photon linear collider, a more detailed analysis is certainly needed. In order to evaluate further a PLC's ability to discover an intermediate-mass Higgs boson, we performed a Monte Carlo simulation of an experiment at a PLC. The differential $\gamma\gamma$ luminosity of Fig. 11 is folded in with the relevant cross sections in a Monte Carlo event generator. The resulting generated partons are fragmented into jets using JETSET 6.3 (LUND) [28] and the events processed through the Fast Monte Carlo simulation of the SLC Large Detector (SLD) at SLAC [29]; the relevant detector parameters are summarized in Table I.

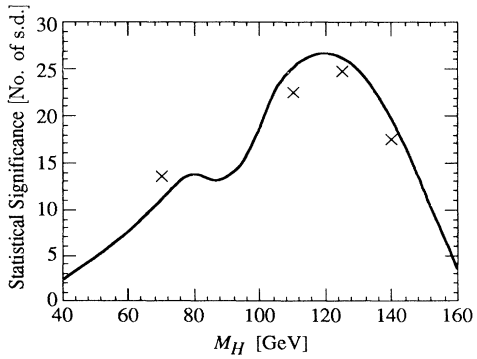

FIG. 13. Statistical significance of the Higgs boson signal given the event rates in Fig. 12. 50% $b\bar{b}$ tagging with 5% $c\bar{c}$ contamination is assumed, as well as a Gaussian reconstruction resolution with FWHM$=0.1W_{\gamma\gamma}$. The $\times$'s result from the Monte Carlo simulation shown in FIG. 14.

TABLE I. Important SLD specifications.

Tracking	Drift chamber
Magnetic field	0.6 T
Momentum resolution ($\delta p/p$)	0.0015 (p/GeV)⊕0.01
Two-track separation	1.0 mm
Electromagnetic calorimetry	Lead/liquid argon
Depth	22 radiation lengths
Energy resolution ($\delta E/E$)	$8\%/\sqrt{E/\text{GeV}}$
Segmentation	33 mrad×36 mrad
Angular resolution	5 mrad
Hadronic calorimetry	Lead/liquid argon + iron/gas
Depth	7 interaction lengths
Energy resolution ($\delta E/E$)	$55\%/\sqrt{E/\text{GeV}}$
Segmentation	66 mrad×72 mrad
Angular resolution	10 mrad
Vertexing	Silicon pixel charge-coupled device
Particle identification	Cherenkov ring imaging device

After selecting two-jet events (defined by the JADE algorithm [30]) and making a cut on the center-of-mass thrust angle, the invariant mass of each event was reconstructed. We did not simulate vertexing and particle identification to tag the b quarks, but put in the $b\bar{b}$ and $c\bar{c}$ efficiencies by hand.

A histogram of invariant masses is plotted in Fig. 14, revealing the resonant Higgs boson above the continuum background. The Higgs boson signal is clearly evident for all masses in the region of interest. The peak near 90 GeV results from untagged two-fermion production of Z bosons. The statistical significance of the Higgs boson signal at each of the four masses is indicated in Fig. 13. Note that the SLD detector used in this simulation is not optimized for Higgs boson physics; a detector optimized for jet-jet mass reconstruction would do considerably better.

The high statistical significance of the Higgs boson signal, demonstrated in Figs. 13 and 14, is obtained through excellent suppression of the continuum background underneath the Higgs boson signal. This suppression was achieved in two ways: high linac polarization leading to very polarized photon beams, and good rejection of $c\bar{c}$ events. Figure 15 shows how the statistical significance of the signal varies as a function of these two parameters. It is obvious that one should strive for as high a linac polarization as possible, and a $c\bar{c}$-to-$b\bar{b}$ acceptance ratio below a few percent in order to maximize the statistical significance of the Higgs boson signal.

Systematic errors, at least for the issue of discovery, should be unimportant, except for the case in which the Higgs boson mass is very near that of the Z. In that case, an accurate determination of the number of Z events will be needed, so as to be able to infer an excess. This determination will have to come from measurement and Monte Carlo simulation. This may prove to be difficult, since easily identified decay modes of the Z, such as leptonic modes, ride on a very large continuum background. Thus, less easily identified decay modes which have lower backgrounds, such as $s\bar{s}$, will need to be used. In any case, this method of discovering a Higgs boson with a mass very near that of the Z will most probably by systematics limited. However, if there were any indication of a Higgs boson signal near 91 GeV, the appropriate strategy would be to switch to a more peaked $\gamma\gamma$ lumi-

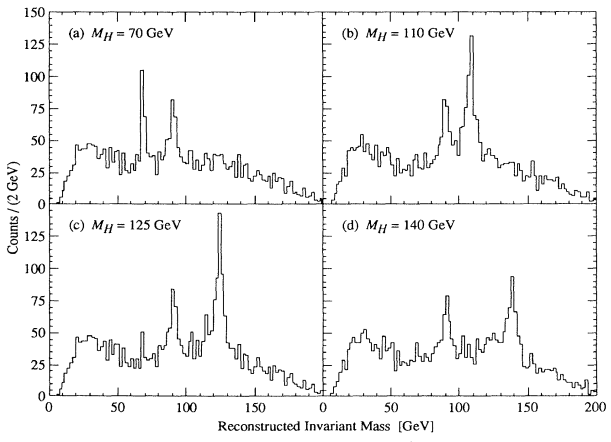

FIG. 14. Results of a Monte Carlo simulation of a search for an intermediate-mass Higgs boson at a photon linear collider. The luminosity spectrum used is that of Fig. 11. 50% $b\bar{b}$ tagging with 5% $c\bar{c}$ contamination is assumed, and a cut of $|\cos\theta| < 0.7$ is employed. The peak at 90 GeV results from untagged two-fermion production of Z bosons.

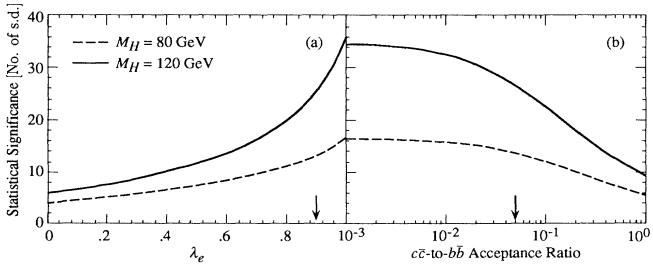

FIG. 15. The statistical significance of the Higgs boson signal as a function of linac polarization and charm contamination. In each plot all other parameters are as in Fig. 13; the arrows indicate the values assumed in Figs. 13 and 14.

nosity distribution, which would greatly increase the signal-to-background ratio.

V. HIGGS BOSON STUDY AT A PLC

Once one, or several, Higgs bosons are found, their properties must be determined. A photon linear collider offers a unique environment in which to measure the two-photon width of a Higgs boson once found. As can be seen from Eq. (5), measuring the production rate in $\gamma\gamma$ collisions of exclusive Higgs boson events determines the product of the two-photon width of the Higgs boson and its branching ratio to the detected final state. This product can then be compared to the predictions of various models, or the width can be extracted by independently measuring the branching ratio to $b\bar{b}$ or ZZ (at, for example, an e^+e^- collider).

For the purposes of measuring the two-photon width, the peaked luminosity distribution, obtained by using the $\lambda_e\lambda_\gamma<0$, $\rho>1$ configuration is most suited [see Fig. 6(b)]. In this configuration, the luminosity distribution is fairly monochromatic ($\sim 10\%$ energy spread) and very highly polarized ($>95\%$), resulting in a high signal-to-background ratio. We choose a ρ parameter of 3.0 to suppress sufficiently the low mass luminosity. Figure 16 shows the resulting $\gamma\gamma$ luminosity, broken down into its helicity components and assuming 20 fb^{-1} of effective luminosity.

Of course, the collider energy must be tuned so that the peak of the luminosity spectrum sits at the Higgs boson mass. Fortunately, planned linear colliders are being designed to be operated at any energy below their maximum [31]. This flexibility will ensure the accessibility of any Higgs boson with mass in the intermediate or heavy region (assuming that the energy reach of the collider is sufficient).

Plotted in Fig. 17 are expected event rates for both the signal and background processes, given the luminosity distribution of Fig. 16; only $b\bar{b}$ and ZZ final states are included. It is assumed that (for $H\to b\bar{b}$) a window in invariant mass of $\pm 2\sigma$ around the Higgs mass is used for the measurement and that the reconstruction resolution

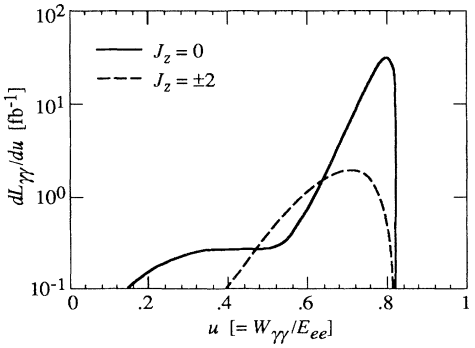

FIG. 16. The $\gamma\gamma$ luminosity distribution to be used in a measurement of the two-photon width of a Higgs boson. 90% linac polarization, a ρ value of 3.0, and 20 fb^{-1} of integrated effective luminosity are assumed.

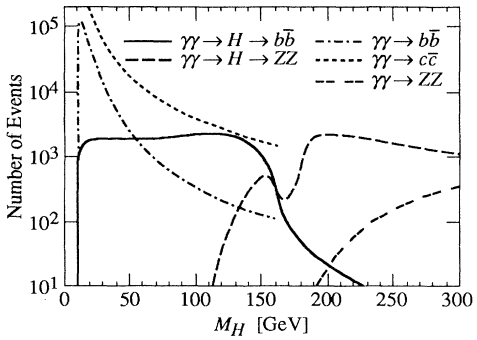

FIG. 17. Expected number of signal and background events for an experiment designed to measure the two-photon width of a Higgs boson. The luminosity distribution of Fig. 16 is used. For the $b\bar{b}$ final state, a cut on production angle of $|\cos\theta|<0.7$ is included.

is Gaussian with FWHM $=0.1M_H$. Note that for Higgs bosons with mass near that of the Z, the background from two-fermion Z production is totally unimportant, as there is essentially no $\gamma\gamma$ luminosity above the peak.

Figure 18 gives the expected statistical error in the measurement of the two-photon width of the Higgs boson. For the $b\bar{b}$ final state, 50% $b\bar{b}$-tagging efficiency with 5% $c\bar{c}$ contamination is assumed. For the ZZ final state, we require one Z to decay to e^+e^- or $\mu^+\mu^-$ and the other to decay visibly (i.e., no $\nu\bar{\nu}$ decays). Monte Carlo studies indicate such a final state is detected with $\sim 80\%$ efficiency; this efficiency is also included in Fig. 18. It is clear that with 20 fb^{-1} of integrated effective luminosity the two-photon width of the Higgs boson can be measured to within 5% over the intermediate-mass range. For heavy-mass Higgs bosons, a 10% measurement is possible, except near WW threshold, where an uncertainty of 20% is expected.

Monte Carlo studies back up the above analysis. Plotted in Fig. 19 is the result of a simulation of an experiment measuring the two-photon width of a 100 GeV Higgs boson, again using the Fast Monte Carlo simulation of the SLD to model the detector response. The

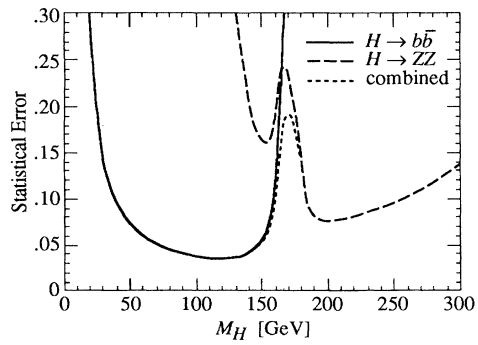

FIG. 18. The statistical error on $\Gamma(H\to\gamma\gamma)$ given the event rates of Fig. 17.

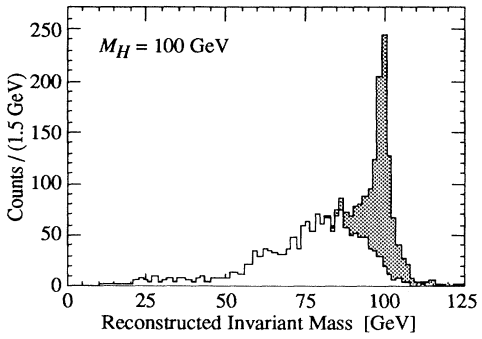

FIG. 19. A Monte Carlo simulation of Higgs boson production for the measurement of the two-photon width of a 100 GeV Higgs boson at a photon linear collider. The luminosity distribution of Fig. 16 is used. The shaded region is the signal, the unshaded is the background.

shaded region is the signal, the unshaded is the background. The statistical uncertainty on the two-photon width in this experiment is 4.7%, consistent with Fig. 18.

As can be seen from Fig. 19 the background under the signal is quite small; the statistical uncertainty in the extracted width is due mostly to the Poisson statistics of the signal itself. At lower linac polarization and with more charm contamination, the background will begin to grow and will contribute to the uncertainty. The statistical uncertainty in the measurement, however, is much less sensitive to these parameters than the statistical significance was in the "search mode." Figure 20 shows the dependence of the statistical error on the linac polarization and $c\bar{c}$-to-$b\bar{b}$ acceptance ratio. It is evident that a precise measurement is possible with just moderate linac polarization and with significant charm contamination.

Systematic uncertainties in the measurement of the product $\Gamma(H\to\gamma\gamma)\times B(H\to b\bar{b},ZZ)$ will be dominated by uncertainties in the efficiency for tagging $b\bar{b}$ or ZZ events. It should be possible to measure the $b\bar{b}$-tagging efficiency using continuum events; ZZ-tagging efficiency should also be well understood using Monte Carlo simulation. A model-independent determination of the two-photon width alone will require a measurement of the branching ratio to the relevant final state, adding an additional systematic error. In an e^+e^- experiment, these branching ratios will be measurable to 5–10% [32], comparable with the statistical uncertainty from the $\gamma\gamma$ experiment.

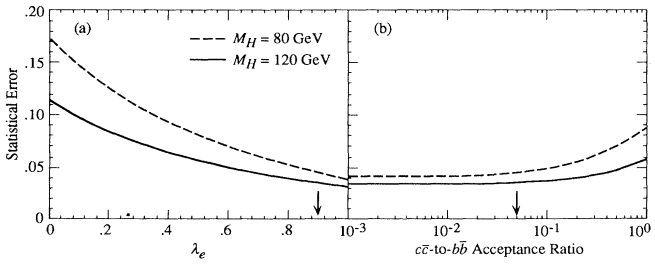

FIG. 20. The statistical uncertainty of the extracted two-photon width as a function of linac polarization and charm contamination. In each plot all other parameters are the same as those used for Fig. 18; the arrows indicate the values assumed for Figs. 18 and 19.

VI. SUMMARY AND CONCLUSION

A photon linear collider capable of high-energy $\gamma\gamma$ collisions provides a unique opportunity to explore the spontaneous symmetry-breaking sector of the standard model, serving as a tool to search for and study Higgs bosons. With linac electron and laser polarization parameters chosen to give a broad luminosity distribution, a $\gamma\gamma$ collider provides a way to search for an intermediate-mass Higgs boson as a resonance in $\gamma\gamma\to b\bar{b}$ production. In such a scheme, the resulting high degree of photon polarization produces a significant reduction of the continuum background and an enhancement of the resonant Higgs boson signal. Given 20 fb^{-1} of effective luminosity, signals with statistical significance of at least 10σ are expected over the entire intermediate-mass range. Crucial to such a search will be highly polarized electron beams (near 90%) to generate polarized $\gamma\gamma$ collisions, excellent vertexing and flavor tagging to reduce the background from charm and light quarks, a strong magnetic field around the interaction point to sweep aside the residual electrons so as to eliminate $e\gamma\to eZ\to(e)b\bar{b}$ as a background to a ~91 GeV Higgs boson, and good hadronic jet reconstruction in the detector.

The search for a Higgs boson must be followed by a program to study its nature. A $\gamma\gamma$ collider provides a singular opportunity to measure one of the most important properties of a Higgs boson. With polarization parameters chosen to give a more monochromatic spectrum, a $\gamma\gamma$ collider makes possible a precise measurement of the two-photon width of the Higgs boson, providing an opportunity to discriminate among various competing models of spontaneous symmetry breaking. With 20 fb^{-1} of effective luminosity, a measurement of the two-photon width of the Higgs boson can be made with a statistical precision of better than 5% over the intermediate-mass range using $\gamma\gamma\to H\to b\bar{b}$, and 10% for higher masses using $\gamma\gamma\to H\to ZZ$. Although beneficial, very high linac polarization and superb charm rejection are not crucial to such a measurement.

ACKNOWLEDGMENTS

We would like to acknowledge valuable discussions with Tim Barklow, Chris Bowdery, Chris Damerell, Ilya Ginzburg, Mike Hildreth, Valery Khoze, and Valery Telnov. We would like to express sincere gratitude to Mike Strauss and Richard Dubois for their assistance with the Monte Carlo simulation of the SLD detector. We would like to thank George Jikia for providing us with his code to calculate $\gamma\gamma\to ZZ$ cross sections, and Howard Haber for his code to calculate Higgs boson masses and decay widths in the MSSM. This work was supported in part by Department of Energy under Grant No. DOE-FG-91ER40618. One of us (D.L.B.) was supported in part by the National Science Foundation.

[1] Particle Data Group, K. Hikasa *et al.*, Phys. Rev. D **45**, S1 (1992).
[2] J. F. Gunion *et al.*, *The Higgs Hunters Guide, Frontiers in Physics Series* Vol. 80 (Addison-Wesley, Redwood City, CA, 1990).
[3] M. Schneegans, in *1991 Electroweak Interactions and Unified Theories,* Proceedings of the Leptonic Section of Rencontres de Moriond, Les Arcs, France, 1991, edited by J. Tran Thanh Van (Editions Frontieres, Gif-sur-Yvette, France, 1991), p. 473; Z. Kunszt *et al.*, Phys. Lett. B **271**, 247 (1991).
[4] B. Ioffe and V. Khoze, Fiz. Elem. Chastits At. Yadra **9**, 118 (1978) [Sov. J. Part. Nucl. **9**, 50 (1978)]; J. Ellis, M. K. Gaillard, and D. V. Nanopoulos, Nucl. Phys. **B106**, 292 (1976).
[5] D. R. T. Jones and S. T. Petcov, Phys. Lett. **84B**, 440 (1979).
[6] Y. Okada *et al.*, Prog. Theor. Phys. **85**, 1 (1991); H. E. Haber and R. Hempfling, Phys. Rev. Lett. **66**, 1815 (1991); J. Ellis *et al.*, Phys. Lett. B **257**, 83 (1991).
[7] J. F. Gunion and H. E. Haber, in *Research Directions for the Decade,* Proceedings of the Summer Study on High Energy Physics, Snowmass, Colorado, 1990, edited by E. L. Berger (World Scientific, Singapore, 1992), p. 469.
[8] H. König, Phys. Rev. D **45**, 1575 (1992).
[9] Figure 3 was generated with the aid of a computer program supplied to us by H. Haber.
[10] Z. Kunszt and F. Zwirner, Nucl. Phys. **B385**, 3 (1992).
[11] I. F. Ginzburg *et al.*, Nucl. Instrum. Methods **205**, 47 (1983); I. F. Ginzburg *et al.*, *ibid.* **219**, 5 (1984).
[12] V. I. Telnov, Nucl. Instrum. Methods **A294**, 72 (1990).
[13] D. L. Borden, D. A. Bauer, and D. O. Caldwell, Report No. SLAC-PUB-5715, 1992 (unpublished); Report No. UCSB-HEP-92-01, 1992 (unpublished).
[14] V. I. Telnov and P. Chen, Phys. Rev. Lett. **63**, 1796 (1989).
[15] R. Ruth, in *Physics and Experiments with Linear Colliders,* Proceedings of the Workshop, Saariselkä, Finland, 1991, edited by R. Orava *et al.* (World Scientific, Singapore, 1992), p. 629; G. Voss, *ibid.*, p. 777.
[16] J. B. Rosenzweig, in Proceedings of the First International TESLA Workshop, Ithaca, New York, edited by H. Padamsee, Cornell, 1990, p. 180; M. Tigner, in *Physics and Experiments with Linear Colliders* [15], p. 705.
[17] K. A. Isparin *et al.*, Yad. Fiz. **11**, 1278 (1970) [Sov. J. Nucl. Phys. **11**, 712 (1970)]; T. Barklow, in *Research Directions for the Decade* [7], p. 440.
[18] M. Drees *et al.*, Phys. Lett. B **306**, 371 (1993).
[19] O. J. P. Éboli *et al.*, Phys. Rev. D **48**, 1430 (1993).
[20] L. F. Landau, Dokl. Akad. Nauk USSR **60**, 207 (1948); C. N. Yang, Phys. Rev. **77**, 242 (1950).
[21] G. Jikia, Report No. IHEP-93-37, 1993 (unpublished); in Proceedings of the 1993 Workshop in Physics and Experiments with Linear e^+e^- Colliders, Waikoloa, Hawaii (unpublished).
[22] I. F. Ginzburg and V. G. Serbo, in Proceedings of the 1993 Workshop in Physics and Experiments with Linear e^+e^- Colliders [21].
[23] E. Yehudai, Phys. Rev. D **44**, 3434 (1991).
[24] D. Bowser-Chao and K. Cheung, Phys. Rev. D **48**, 59 (1993).
[25] T. Maruyama *et al.*, Phys. Rev. Lett. **66**, 2376 (1991).
[26] T. Nakanishi *et al.*, Report No. DPNU-91-23, 1991 (unpublished); T. Nakanishi *et al.*, in *1991 IEEE Particle Accelerator Conference: Accelerator Science and Technology,* Proceedings of the Conference, San Francisco, California, 1991 (IEEE, Piscataway, New Jersey, 1991), p. 2032.
[27] C. Damerell and C. Bowdery (private communication).
[28] T. Sjöstrand, Comput. Phys. Commun. **27**, 243 (1982); **39**, 3473 (1986); T. Sjöstrand and M. Bengtsson, *ibid.* **43**, 367 (1987).
[29] SLD Design Report No. SLAC-0273 (unpublished); M. Breidenbach, Nucl. Sci. Symp. **46** (1985).
[30] JADE Collaboration, W. Bartel *et al.*, Z. Phys. C **26**, 93 (1984).
[31] T. Omori, in the Proceedings of the 1993 Workshop in Physics and Experiments with Linear e^+e^- Colliders [21].
[32] M. Hildreth, in Proceedings of the Workshop on Electroweak Symmetry Breaking at Colliding-Beam Facilities, Santa Cruz, California, 1992 (unpublished).